Am. Math. Soc. 48, 739 (1942).
[30]N. L. Peterson and S. J. Rothman (private communication).
[31]Y. Shimomura, Phil. Mag. 19, 773 (1969).

PHYSICAL REVIEW B VOLUME 3, NUMBER 4 15 FEBRUARY 1971

Magnetoacoustic Absorption of Longitudinal Sound in Magnesium in High Magnetic Fields†*

Robert W. Reed and F. G. Brickwedde
Department of Physics, The Pennsylvania State University, University Park, Pennsylvania 16802
(Received 10 June 1970)

Pulse-echo measurements were made of the oscillations in the attenuation of 100–420 MHz longitudinal sound in single crystals of Mg [99.95%; $R(300\text{ K})/R(4.2\text{ K}) \sim 425$]. The $\vec{q}$ in different specimens was parallel to the [0001], [11$\bar{2}$0], and [10$\bar{1}$0] axes; H was varied from 1 to 40 kOe. The temperature was varied from 1 to 4.2 K, and ql from 0.4 to 1.8. Areas of extremal-sized cross sections of the Fermi surface, oriented perpendicular to $\vec{H}$, were calculated from the $\Delta(1/H)$ periods in attenuation. These areas are in good agreement with Stark's values from de Haas–van Alphen–effect data using much purer Mg, with the exception of the μ_1^5 area, where there is a 2% difference. The short $\Delta(1/H)$-period magnetoacoustic oscillations corresponding to the large-area λ_1^4 oscillations were modulated with the long period corresponding to the small μ_1^5 area, and the λ_2^4 oscillation was modulated with the period corresponding to the μ_2^4 area. This phenomenon is not satisfactorily explained. A simple derivation is given for magnetoacoustic oscillations (periods and amplitudes) on the assumption that the only effect of $\vec{H}$ on the attenuation is through its effect on the density of states at the Fermi surface. The de Haas–van Alphen ($ql < 0.7$) and intermediate ($ql > 0.7$) regions of magnetoacoustic absorption are included. The dependence of the oscillation amplitudes on H, T, τ, ql, and the direction of $\vec{q}$ was checked experimentally.

I. INTRODUCTION

This is a report on the investigation of the oscillations in the magnetoacoustic (MA) absorption of longitudinal sound in single crystals of Mg as $\vec{H}$ was varied in magnitude and direction. The investigation was carried out with 100–420 MHz sound, at temperatures between 1.0 and 4.2 K, in fields from 1 to 40 kOe, using single crystals[1] of Mg having resistance ratios between 350 and 450. The product ql (q is the sonic wave number $2\pi/\lambda$, and l is the electron mean free path) in our investigation was of order 1. This puts our investigation in a region of ql in which the oscillations in the ultrasonic attenuation coefficient $\alpha(B)$ have an origin similar to the origin of the oscillations of the magnetic susceptibility in the de Haas–van Alpen (dHvA) effect. As a consequence, the MA oscillations we observed were similar in frequency, temperature and field dependence of amplitude, and line shape to the oscillations in the dHvA effect.

The MA oscillations in $\alpha(B)$ are periodic in $1/B$. The $1/B$ periods are proportional to reciprocals of extremal values of the cross-sectional areas of the Fermi surface (FS) in k space sectioned by planes perpendicular to $\vec{B}$. The areas are extremal with respect to displacements of the intersecting plane along the axis of $\vec{B}$. The FS is oriented with respect to the crystal axes; by varying the orientation of the axes of a crystal with respect to the solenoid field $\vec{H}$, extremal areas for all orientations relative to the crystal axes are, in principle, obtainable. The extremal areas, in conjunction with theoretically determined electron band structures and electron constant-energy surfaces in $\vec{k}$ space, make possible determinations of the actual shape and size of the FS, and with this information to calculate a *pseudopotential* for the conduction electrons.[2]

The FS of Mg has been investigated experimentally by others and by other methods.[3–7] The most recent and complete measurements on Mg are the MA measurements of the geometric-resonance type ($ql \gg 1$) by Ketterson and Stark,[8] and the dHvA-effect measurements by Stark.[9] Our MA data (extremal cross sections of the FS) are compared with accurate data by Stark[9] from dHvA measurements. The labeling of cross sections of the FS in our paper was adopted from Stark.[9]

A theory for MA oscillations is presented for the region $\omega\tau \ll 1$ (ω is the sonic angular frequency, τ is the relaxation time for an electron). The ideas and mathematics are not original, but as far as we are aware, the theory for MA absorption in the $\omega\tau \ll 1$ region has not been presented before in the mathematically simple method followed here.

We investigated experimentally the dependence of

the amplitude of the MA oscillations in our Mg specimens on T, B, ql, τ, and the direction of $\vec{q}$, and compared the results with our theoretical equation (12) which is in agreement with the observations.

II. THEORY

Equations for Landau-level oscillations in the absorption $\alpha(\vec{q}, l, \vec{B})$ of beams of longitudinal sound in metals have been derived by different authors using different assumptions and mathematical methods.[10–13] The equations obtained agree with respect to the MA frequencies, but differ with respect to the amplitudes of the oscillations.

It is evident from (i) the theories for MA oscillations; (ii) similarities between the oscillations in the MA and dHvA affects; (iii) the theory for the dHvA effect; (iv) theories like Pippard's[14] for ultrasonic attenuation by conduction electrons when $B = 0$, that the most significant physical feature responsible for the MA oscillations, in metals in which ql is of the order of 1, must be the oscillations of the density of electron states at the FS in changing magnetic fields – oscillations that are periodic in $1/B$. Measurements we have made on Mg, and in part report here in Sec. IV, show that the effect of B on other properties that influence the MA absorption are an order of magnitude less important than the effect on the density of states, particularly as regards the oscillations in $\alpha(B)$.

On this physical basis, we derive the equation for MA oscillations in the dHvA and intermediate regions on the assumption that the only effect of B on sonic-beam absorption is through its effect on the energy density of states $\rho(\epsilon_F)$, at the FS.[11] For a free-electron gas

$$\alpha(\vec{q}, l, \vec{B}) = \alpha(q, l, 0)\left(1 + \frac{\rho(\epsilon_F, B) - \rho(\epsilon_F, 0)}{\rho(\epsilon_F, 0)}\right), \quad (1)$$

where $\rho(\epsilon_F, B)$ and $\rho(\epsilon_F, 0)$ are the energy densities of those particular electron states at the FS in which an electron may absorb a sonic-beam phonon. For $\alpha(q, l, 0)$, we have Pippard's equation[15] for an isotropic free-electron gas in zero magnetic field,

$$\alpha(q, l, 0) = \frac{nm}{Mv_s\tau}\left(\frac{q^2l^2\tan^{-1}ql}{3(ql - \tan^{-1}ql)} - 1\right) \equiv \frac{nm}{Mv_s\tau}\,\psi(ql), \quad (2)$$

where n is the number density of electrons of mass m, M is the mass density of metal, v_s is the speed of longitudinal sound, and τ is the electron relaxation time.

At fields greater than 1 kG, ω_c is generally greater than ω, and the cyclotron energy is not altered by the absorption of a phonon. There is an uncertainty in the k_z value of an electron, by reason of the finiteness of its l, equal to

$$\pm(2l\cos\angle\vec{k}, \vec{B})^{-1} = \pm k_F/2lk_z .$$

The equation for conservation of energy and of momentum in the k_z direction parallel to $\vec{B}$, with the uncertainty included, is

$$\hbar^2\left(k_z \pm \frac{1}{2l_z}\right)^2 \Big/ 2m + \hbar\omega = \hbar^2\left(k_z + q_z \pm \frac{1}{2l_z}\right)^2 \Big/ 2m , \quad (3)$$

whence

$$k_z \pm \frac{1}{2l_z} = \left(\frac{mv_s}{\hbar\cos\theta} - \frac{q_z}{2}\right) \pm \frac{k_F}{\sqrt{2}\,q_z l} . \quad (4)$$

Here, $\theta \equiv \angle\,\vec{q}, \vec{H}$, and the $\pm$ signs on opposite sides of (3) are randomly related to each other. Equation (4) states that an electron whose k_z value falls within the range $k_F/\sqrt{2}\,q_z l$ on either side of

$$k_z^0 \equiv [(mv_s/\hbar\cos\theta) - (\tfrac{1}{2}q_z)]$$

may absorb a phonon.[16] For metals with large values of k_F, $(k_z^0/k_F) \ll 1$ except when θ is almost $\frac{1}{2}\pi$, and, in consequence, k_z^0 is considered to be about zero except when θ is almost $\frac{1}{2}\pi$.

If $\sqrt{2}\,q_z l \leq 1$, the dHvA region, electrons with k_z values anywhere on the FS may absorb a sonic-beam phonon, but when

$$1 < \sqrt{2}\,q_z l < 2k_F(\hbar c/eB)^{1/2} ,$$

which characterizes the intermediate region, the electrons that can absorb a sonic-beam phonon are restricted to a range of k_z values, $\pm k_F/\sqrt{2}\,q_z l$, around k_z^0. Hence, for free electrons

$$\rho(\epsilon_F, 0) = \frac{1}{\xi}\left(\frac{V(2m)^{3/2}\epsilon_F^{1/2}}{2\pi^2\hbar^3}\right), \quad (5)$$

where $\xi = 1$ if $\sqrt{2}\,q_z l \lesssim 1$, and $\xi = \sqrt{2}\,q_z l$ if

$$1 < \sqrt{2}\,q_z l < 2k_F(\hbar c/eB)^{1/2}$$

The upper limit on $\sqrt{2}\,q_z l$ for the intermediate region is set by the effective limits $k_z = \pm\frac{1}{2}(eB/\hbar c)^{1/2}$ of the Fresnel-type integral involved in the calculation of the oscillatory part of the Helmholtz free energy, $A_{\rm osc}$, in Eqs. (6) and (10); see, for example, Ziman.[17] The integration extends over the full k_z range of the FS; however, a net contribution comes only from the part that extends from $k_z = -\frac{1}{2}(eB/\hbar c)^{1/2}$ to $+\frac{1}{2}(eB/\hbar c)^{1/2}$ and is centered on the extremal area at $k_z = 0$. Outside these k_z limits, the integrand oscillates rapidly positively and negatively; see, for example, Pippard.[18]

The numerator in Eq. (1) $[\rho(\epsilon_F, B) - \rho(\epsilon_F, 0)]$ is derivable from our Eq. (6), which is from a paper by Brailsford.[19] Here τ is the mean collision time of the electrons in cyclotron orbits at $k_z = 0$:

$$A_{\rm osc} = A(T, V, B) - A(T, V, 0)$$

$$= \frac{2Vk_BT}{\sqrt{2\pi}}\left(\frac{eB}{2\pi\hbar c}\right)^{3/2}\sum_{p=1}^{\infty}\frac{(-1)^p}{p^{3/2}}$$

$$\times\frac{\cos(2\pi pmc\epsilon_F/\hbar eB-\frac{1}{4}\pi)\,e^{-\pi pmc/eB\tau}}{\sinh(2\pi^2 pmck_BT/\hbar eB)}\ . \quad (6)$$

In Eq. (6), ϵ_F is the Fermi energy of an "impure" metal. For free electrons, $\epsilon_F(B=0)$ is sensitive only to changes in the density of the conduction electrons, which can result from changes in lattice parameters or from changes in the average valence $\bar{v}$ of the metal, in which case $\epsilon_F(i)$ for the impure metal is equal to $\epsilon_F(0)+[x\Delta\bar{v}/\rho(\epsilon_F,0)]$, where x is the atomic concentration of the impurities.

The following thermodynamic relations are used in the calculation from A of ρ, the energy density of electron states: (a) the equation

$$\left(\frac{dA}{d\mu}\right)_{T,V,B}=nV-\beta^{-1}\left(\frac{d\ln\mathfrak{Q}(z,V,B,T)}{d\mu}\right)_{T,V,B}=0\ ,$$

which is used to calculate $n(\epsilon_F,T,B)$, the density of electrons; μ (chemical potential) $=\epsilon_F$; $z\equiv e^{\beta\mu}$; $\beta=1/k_BT$; $\mathfrak{Q}$ (grand partition function) $=\prod_s\times(1+ze^{-\beta\epsilon_s})$;

$$\epsilon_s=(\lambda_s+\tfrac{1}{2})\hbar\omega_c+(\hbar^2k_{z,s}^2/2m)\ ;$$

and (b) the equation

$$\left(\frac{\partial n(\epsilon_F,T,B)}{\partial\epsilon_F}\right)_{T,B}=\rho(\epsilon_F,T,B)\ ,$$

assuming that $k_BT\ll\epsilon_F$;

$$\rho(\epsilon_F,B)-\rho(\epsilon_F,0)=\frac{2Vk_BTm^2}{\hbar^3}\left(\frac{c}{\hbar eB}\right)^{1/2}\times\sum_{p=1}^{\infty}\frac{(-1)^p p^{1/2}\cos(2\pi mcp\epsilon_F/\hbar eB-\frac{1}{4}\pi)}{\sinh(2\pi^2pmck_BT/\hbar eB)}\times e^{-\pi pmc/eB\tau}\ . \quad (7)$$

Using (7) and (5) in (1), and making the substitutions S_0 (the extremal area of cross section of the FS perpendicular to $\vec{B}$) $=2\pi m\epsilon_F/\hbar^2$, and T_D (Dingle temperature[20]) $\equiv\hbar/2\pi k_B\tau$, we obtain for free electrons

$$\alpha(\vec{q},l,\vec{B})=\alpha(q,l,0)\left[1+\xi\frac{2\pi^2mk_BT}{\hbar}\left(\frac{\pi c}{\hbar eBS_0}\right)^{1/2}\times\sum_{p=1}^{\infty}\frac{(-1)^p p^{1/2}\cos(p\hbar cS_0/eB-\frac{1}{4}\pi)}{\sinh(2\pi^2pmck_BT/\hbar eB)}\times\exp\left(\frac{-2\pi^2pmck_BT_D}{\hbar eB}\right)\right]\ . \quad (8)$$

A general FS is sectioned by Brillouin surfaces, and different sections, or sheets, are isolated by energy barriers. Equation (8), therefore, has to be modified. For a segmented FS, $\alpha(\vec{q},l,\vec{B})$ is resolvable into components $\alpha_j(\vec{q},l,\vec{B})$ arising from different extremal cross sections j of the same or different sheets. MA oscillations occur with different periods and zero-field attenuations $\alpha_j(\vec{q},l,\vec{B}\to0)$. For a particular sheet and the regions bordering a particular cross section of extremal area at $k_z=k_{zf}$, we have in place of Eq. (4)

$$k_z-k_{zj}\pm\frac{1}{2l_z}=\frac{m_{zj}^*v_s}{\hbar\cos\theta}-\frac{q_z}{2}\pm\frac{k'_{F,j}}{\sqrt{2}\,q_zl}\ , \quad (9)$$

where (i) the subscript j refers to the extremal cross section at $k_z=k_{zj}$, perpendicular to $\vec{B}$ (k_z axis); (ii) $(m_{zj}^*)^{-1}=(\partial^2\epsilon/\partial k_z^2)_{k_{zj}}/\hbar^2$; and (iii) k'_{Fj} is the mean radius vector, in the $k_z=k_{zj}$ plane, of the intersection of this plane with the ith sheet. According to Eq. (9), the range of k_z values possible for absorption is $\sim k'_{Fj}/\sqrt{2}\,q_zl$ and is centered on

$$k_z^0\equiv k_{zj}+m_{zj}^*v_s/\hbar\cos\theta-\tfrac{1}{2}q_z\ ,$$

which is $\sim k_{zj}$ except when θ is about $\frac{1}{2}\pi$.

In the dHvA region, *all* electrons of sheet i, cut by section j, can participate. This occurs when $|k_{zj}|\gtrsim|\frac{1}{2}k_{Fi}|$ if

$$\sqrt{2}\,q_zl\lesssim|k'_{Fj}|/|k_{zj}|\ ,$$

and if

$$\sqrt{2}\,q_zl\lesssim|k'_{Fj}|/(|k_{Fi}|-|k_{zj}|)$$

when $|k_{zj}|<|\frac{1}{2}k_{Fi}|$. Here, $2|k_{Fi}|$ is the diameter of the ith sheet in the k_z direction. The density-of-states function $\rho(\epsilon_F,0)$, Eq. (5) for the spherical FS, is replaced by $\rho_i(\epsilon_F,0)$, the density of states for the ith sheet, equal to the integral of $V/8\pi^3(\nabla_{\vec{k}}\epsilon)_{\epsilon_F}$ over the ith sheet of the FS.

The intermediate region extends from the limit of the Fresnel integral, from

$$\sqrt{2}\,q_zl\sim2|k'_{Fj}|(\hbar c/eB)^{1/2}\ ,$$

to the limit of the dHvA region given above. The density $\rho_{ij}(\epsilon_F,\vec{q},l,\hat{k}_z)$ of states that participate in absorption is a function of q_zl and of the orientation of $\vec{B}$ with respect to the crystal axes.

Equation (1) is replaced by (10) for the extremal cross section j:

$$\alpha_j(\vec{q},l,\vec{B})=\alpha_j(\vec{q},l,\vec{B}\to0)\times\left(1+\frac{\rho_j(\epsilon_F,\vec{B})-\rho_j(\epsilon_F,\vec{B}\to0)}{\rho_j(\epsilon_F,\vec{B}\to0)}\right)\ . \quad (10)$$

In place of Eq. (6), use is made of Brailsford's[21] equation for a segmented FS:

$$A_{oscj}=A_j(T,V,\vec{B})-A_j(T,V,0)=\frac{2Vk_BT}{[S''(\epsilon_F,k_{zj})]^{1/2}}\left(\frac{eB}{2\pi\hbar c}\right)^{3/2}\times\sum_{p=1}^{\infty}\left[\frac{\cos(2\pi pm_{cj}^*c\epsilon'_{Fj}/\hbar eB-2\pi p\gamma-\frac{1}{4}\pi)}{p^{3/2}\sinh(2\pi^2pm_{cj}^*ck_BT/\hbar eB)}\right.$$

$$\times \exp\left(\frac{-\pi p m^*_{cj} c}{eB\tau_j}\right)\Bigg], \qquad (11)$$

where (a) ϵ_F is for a metal with "impurities"; (b) $\epsilon'_{Fj} = \epsilon_F - \hbar^2 k_{zj}^2/2m^*_{zj}$; (c) taking $S(\epsilon_F, k_{zj})$ as the area cross section of the FS at k_{zj} perpendicular to $\vec{B}$,

$$m^*_{cj} = \frac{\hbar^2}{2\pi}\left(\frac{\partial S(\epsilon, k_z)}{\partial \epsilon}\right)_{\epsilon_F, k_{zj}};$$

(d) $S(\epsilon, k_z) = (\lambda+\gamma)(2\pi eB/\hbar c)$ and

$$S''(\epsilon_F, k_{zj}) = \left(\frac{d^2 S}{dk_z^2}\right)_{\epsilon_F, k_{zj}};$$

and (e) $\epsilon = (\lambda+\gamma)\hbar\omega_c + \hbar^2 k_z^2/2m^*_z$. For free electrons, $S'' = 2\pi$ and $\gamma = \frac{1}{2}$.

For each *extremal* cross section S_{ij} of sheet i, there is a characteristic equation (11) for $A_{\mathrm{osc}j}$ and a characteristic equation for $\alpha_{ij}(\vec{q}, l, \vec{B})$;

$$\alpha_{ij}(\vec{q}, l, \vec{B}) = \alpha_{ij}(\vec{q}, l, \vec{B}\to 0)\Bigg[1 + \frac{\sqrt{2}\, q_z l}{\phi_{ij}(\epsilon_F, \vec{q}, l, \hat{k}_z)} \times \frac{2k_B T m^*_{cj} V}{\hbar^3 [S''(\epsilon_F, k_{zj})]^{1/2}}\left(\frac{2\pi c}{\hbar eB}\right)^{1/2} \times \sum_{p=1}^{\infty} \frac{p^{1/2}\cos(p\hbar c S_{ij}/eB - 2\pi p\gamma - \frac{1}{4}\pi)}{\sinh(2\pi^2 p m^*_{cj} c k_B T/\hbar eB)} \times \exp\left(\frac{-\pi p m^*_{cj} c}{eB\tau_j}\right)\Bigg]. \qquad (12)$$

Here, $\phi_{ij}(\epsilon_F, \vec{q}, l, \hat{k}_z)$ is a function introduced for convenience and is by definition equal to $\sqrt{2}\, q_z l \rho_{ij}(\epsilon_F, \vec{q}, l, \hat{k}_z)$.

In the dHvA region, ϕ_{ij} is $\sqrt{2}\, q_z l\, \rho_i(\epsilon_F, 0)$, where $\rho_i(\epsilon_F, 0)$ is for the whole sheet i of FS at $B = 0$. In the intermediate region, the electrons that participate in absorption cover only part of sheet i.

According to Eq. (12), the absolute amplitude of the oscillations in $\alpha_{ij}(\vec{q}, l, \vec{B})$ arising from the extremal cross section S_{ij} at k_{zj} is the product of $\alpha_{ij}(\vec{q}, l, \vec{B}\to 0)$ and the coefficient of $\cos(p\hbar c S_{ij}/eB - 2\pi p\gamma - \frac{1}{4}\pi)$. As l is decreased, the absolute amplitude decreases because (i) $\alpha_{ij}(\vec{q}, l, \vec{B}\to 0)\to 0$ as $ql \to 0$ [see Eq. (2)]; and (ii) $\tau_j \to 0$, or $T_D \to \infty$. This applies to both the dHvA and intermediate regions, but in the intermediate region there is in addition the factor $\sqrt{2}\, q_z l$ that decreases with l.

Equations (8) and (12), derived here on the basis that the only effect of B in MA absorption of longitudinal sound is through its effect on the density of states at the FS, are in agreement with equations of Skobov[12] and Liu and Toxen[11] using more elaborate methods of calculation, except their equations do not contain the exponential Dingle (T_D or τ_D) factor for the impurity broadening of the Landau levels, and for a factor of 3 in the relative amplitude term.

III. EXPERIMENTAL APPARATUS AND PROCEDURE

The ultrasonic attenuation was measured using a pulse-echo technique[22] employing sonic frequencies in the range 100–420 MHz. A *single-ended* system was used, whereby a single transducer served to excite and receive the ultrasonic waves in the Mg specimens.

Figure 1 is a block diagram of the electronic components of the ultrasonic apparatus. $2\frac{1}{2}$-kW pulses of rf power 1.0 μsec wide were generated with an American Microwave Laboratories, Inc., model 1223 cavity oscillator at a repetition rate of 1 kHz. A 3-dB hybrid junction (Narda model No. 3029) was used to achieve 25-dB isolation between the pulsed oscillator and the receiver. The rf preamplifier[23] withstood the leakage signal through the hybrid junction and gave an order-of-magnitude improvement in the signal-to-noise ratio over the same receiver without the rf preamplifier. Without this preamplifier, measurements above 200 MHz were not possible. The preamplifier was constructed with a low-noise planar triode in conjunction with a tunable cavity. The diode switch (American Electronic Laboratories, Inc. model SNB878A) reduced the leakage pulse by 50 dB before the signal entered the i.f. section of the receiver. Without the diode switch, the i.f. amplifier was paralyzed by leakage from the pulsed oscillator. Placing the diode switch after the rf preamplifier results in a better receiver configuration because of the very-low-noise figure of the rf preamplifier.

A typical balanced mixer i.f. amplifier and local oscillator were used in the receiver. The i.f. amplifier supplied a maximum output of 2 V, which was

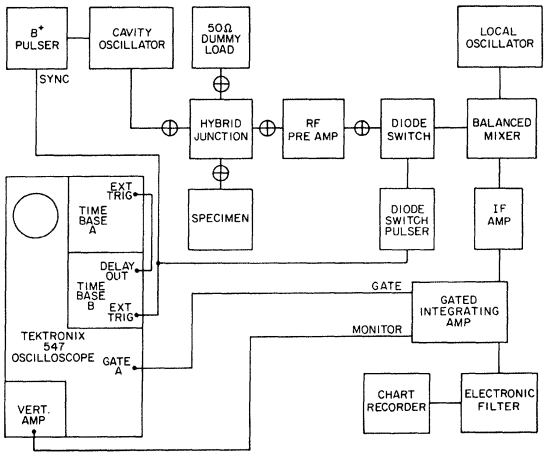

FIG. 1. Block diagram of electronic apparatus. The circles with a plus sign inside indicate a combination of a stub tuner and line stretcher.

sufficient to drive the gated integrating amplifier[24] (a gated amplifier and integrating network) to a 10-V output. This gated integrating amplifier selected a single echo for continuous recording. It was designed for (a) a time constant of less than 1 μsec for charging the capacitors in the integrating network; (b) a choice of time constants from 0.5 to 40 sec for discharging the capacitors; and (c) drifts, with time and changes of room temperature, in output voltage of less than 0.5%. The signal from the gated integrating amplifier (0–10 V) was passed through two low-frequency bandpass filters (Krohn-Hite models 330BR and 3342) connected in series for discrimination between concurrent oscillations of different frequencies in the ultrasonic attenuation in a specimen. The frequencies encountered depended on the $1/H$ rate of sweep of the magnetic field and ranged from 0.02 to 0.5 Hz.

The output of the electronic filters was continuously recorded with a Mosely model No. 7101BM strip-chart recorder. Magnet currents were indicated on the edge of the chart with a second pen.

Disk-shaped specimens, about 1 cm in diameter and 0.2–0.3 cm thick, were acid-string-saw[25] cut from three large single crystals[1] of Mg. Specimens were cut with disk faces perpendicular to the [0001], [10$\bar{1}$0], and [11$\bar{2}$0] axes. The orientation error, that resulted because the string saw did not cut accurately perpendicular to the desired axis, did not exceed 3° as determined by back-reflection x-ray Laue photographs.

The specimens were lapped on silicon-carbide paper, using grits from No. 400 to No. 600. It was found that covering the silicon-carbide paper with a 6% solution of HCl greatly reduced distortion at the surface of the specimens. Electropolishing following the lapping produced mirrorlike surfaces. These electropolished specimens exhibited less ultrasonic attenuation, which was attributed to less sonic scattering at the specimen surfaces.

The specimens were bonded between a 20-MHz wrap-around coaxially plated X-cut quartz transducer and a Z-cut quartz delay rod 1 cm long and 0.945 cm in diameter. General Electric silicone-rubber adhesive "Clear Seal" was used as the bonding agent. A bonding press similar to that described by Levy and Rudnick[26] was used. The adhesive was cured at room temperature from 3 to 5 days under a weight of 2 kg.

A prepared Mg specimen was mounted in a rotatable specimen holder inside a 4.3-cm-i.d. metal liquid-helium finger Dewar (see Fig. 2). The axis of rotation of the specimen was horizontal and parallel to the plane of the disk. The direction of $\vec{H}$ was vertical, and the plane in which the specimen axis was rotated was vertical, passing through $\vec{H}$.

The magnetic field was generated with a Varian Associates superconducting magnet and was variable from 0 to 40 kOe.[27] The field was uniform to one part in 10^4 within a 2.5-cm-diam sphere at the center of the magnet, and $1/H$ was linearly variable with respect to time. The magnet current (0–16 A) was determined to the nearest 0.1 mA by measuring the difference of potential across a milliohm resistor in series with the magnet with a Hewlett-Packard model 740B differential voltmeter. The equations relating H to the magnet current were

$$H\,(\text{increasing}) = (2.552I - 0.056)\times 10^3 \text{ Oe}\,,$$
$$H\,(\text{decreasing}) = (2.554I + 0.102)\times 10^3 \text{ Oe}\,, \tag{13}$$

where I is in amperes. These equations were determined empirically using a rotating-coil Rawson Electrical Instrument Co. model 820 gaussmeter calibrated against a Penn State NMR magnetometer. The measurements were made at constant magnet currents. H was measured with an accuracy of 0.1%, and Eqs. (13) were reliable to 0.3% for fields greater than 4 kOe. Equations (13) were checked over a period of 2 yr after many temperature cyclings of the magnet between 4.2 and 77 K. These equations, for constant values of magnet current, had to be modified when the magnet current was swept because the superconducting solenoid was shunted by a persistent-current switch operated in the normal resisting mode. A time-varying flux in the superconducting solenoid induced a current

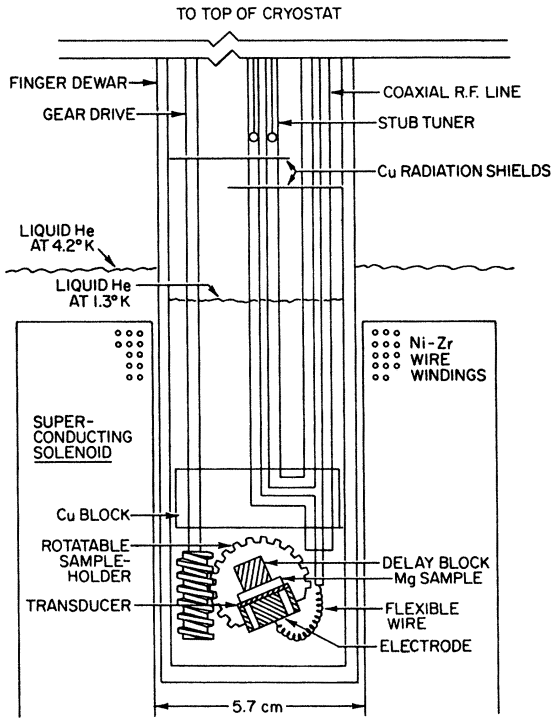

FIG. 2. Diagram of sample holder and superconducting magnet.

in the solenoid, only part of which flowed through the magnet-current measuring resistor because of the shunting by the persistent-current switch. The magnet current $I_m(t)$ during a $1/H$ sweep was related to the current $I_a(t)$ through the milliohm resistor by the equation

$$I_m(t) = I_a + \sum_{n=1}^{\infty} n! \left(\frac{L}{R}\right)^n \frac{F^n}{[I_{a,i}^{-1} + (t - t_i)F]^{n+1}} , \quad (14)$$

where $F = (I_{a,f}^{-1} - I_{a,i}^{-1})/(t_f - t_i)$, the subscripts i and f refer to the initial and final values at the ends of the $1/H$ sweep, L is the inductance of the magnet, and R is the resistance in the persistent-current switch. Equations (13) used with Eq. (14) yielded consistent $\alpha(B)$-vs-B data for up and down sweeps of the field.

The apparatus was designed specifically to determine the frequencies of periodic changes in ultrasonic attenuation. Changes in the height of a single echo gave changes in $\alpha(B)$ on an arbitrary (nonlinear) scale. Oscillations in echo height were definitely observable above the noise level on the strip chart if their peak-to-peak amplitude was 4 mV when the mean pulse height was 8 V. This sensitivity was achieved when the bandpass filters were set to pass a narrow bandwidth, eliminating higher-frequency noise. If the bandpass filters were not used, oscillations on the order of 50 mV peak to peak were needed to definitely exceed the noise level. Oscillations were observed at fields as low as 5 kOe for the largest amplitude oscillations. At 40 kOe, the amplitudes of these oscillations reached 2–5 V peak to peak on a mean echo height of 5–7.5 V.

The accuracy of determining the $\Delta(1/B)$ periods in $\alpha(B)$ oscillations was dependent on (i) the determination of the magnetic field intensity; (ii) the precision positioning on the strip chart of the time of a reading of the magnet current; and (iii) the accuracy of counting oscillations and determining the positions of the $\alpha(B)$-oscillation peaks on the strip charts. We believe that H was calculated with Eqs. (13) and (14) with an accuracy of 0.3%, and the positions of the magnet current readings were recorded and read with a precision of ±1 mm. The two current markings on the strip charts selected for use in the calculations were generally 1–3 m apart. Positions of attenuation peaks were read with a precision of ±0.2 mm, with from 50 to several hundred peaks being included between these current calibration points. It is believed that we determine the $\Delta(1/B)$ periods with an accuracy of ±1%.

A computer was used in the calculation of the $\Delta(1/B)$ periods and the corresponding extremal areas from the strip-chart data. Since dH^{-1}/dt was not exactly constant [see (13) and (14)], the frequency of the oscillations for a given extremal cross section of the FS was not exactly constant over the length of a chart. Since passage of the oscillations through the electronic filters produced phase changes that were frequency dependent, there were changes in phase shifts that displaced $\alpha(B)$ peaks along the chart. These displacements, though small, were included in the calculations as well as the field corrections given by (13) and (14).

Where there were beats, the beat periods were determined. This gave the difference between the periods of two oscillations and the difference between two cross-sectional areas. If the amplitudes of the beat nodes were zero, or very small, the frequencies of the two component oscillations were symmetrical with respect to the carrier frequency $\frac{1}{2}(\nu_1 + \nu_2)$.

When the amplitude at the beat nodes was not small, the carrier frequency was not $\frac{1}{2}(\nu_1 + \nu_2)$ but did fall between ν_1 and ν_2. In these cases, our difference frequencies $(\nu_1 - \nu_2)$ were in agreement with Stark's[9] data to within our experimental accuracy which was 1% of ν. There were complicated interference patterns that did not exhibit beats with constant-beat frequency. These were not resolved or identified.

The periods of oscillations, if not modulated by beats in a complex way, could be determined with an accuracy of 1%. However, this accuracy was marred if the crystal axis deviated from the specimen axis. Orientation errors up to 3° were observed. It was found that the differences between our extremal areas and Stark's, [9] that were explained by a misorientation of a specimen, were consistent for all the areas observed with that specimen.

The orientation error was not restricted to the plane perpendicular to the axis of rotation. When a desired crystal axis was not perpendicular to the axis of rotation, the crystal axis swept out a cone as the specimen was rotated. For $\vec{H}$ along a principal axis, the orientation error did not exceed the cutting error of 3°.

All data were checked for consistency between up and down sweeps of H. Periods in $\alpha(B)$ and extremal areas were checked using different echoes. Our periods were found to be independent of echo number and sonic frequency to within the claimed accuracy of our measurement

IV. EXPERIMENTAL RESULTS

A. Extremal Cross Sections of FS

The areas[28] in atomic units of the extremal cross sections that we measured perpendicular to B are plotted in Fig. 3 as functions of the orientation of $\vec{B}$ in planes determined by two principal crystal axes. The Greek letters refer to different sheets

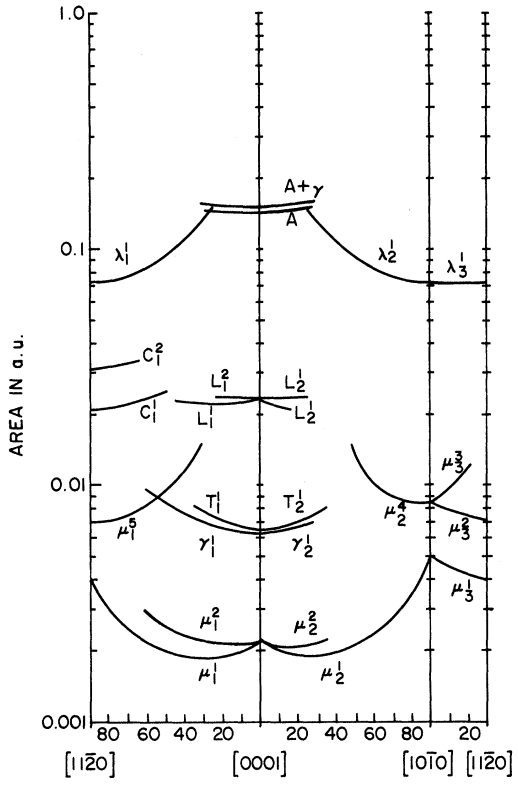

FIG. 3. Composite of the extremal cross-sectional areas of the Fermi surface determined magnetoacoustically versus orientation in degrees. Table I lists the areas along the three crystal axes.

of the FS; μ, γ, and λ refer to cross sections of the monster, cigar, and lens, respectively; see Fig. 4. Capital Roman letters designate extremal areas (normal to $\vec{B}$) encircled by cyclotroning electrons passing over two or more sheets of a FS; for example, the A and $(A+\gamma)$ areas in Fig. 5(e) which couple the waist of the monster and the cigar in different patterns. The cyclotron orbits encircling these Roman-lettered sections are called magnetic breakdown (MB) orbits because the magnetic field promotes "tunneling" by electrons through an energy barrier that separates the different sheets. Breakdown occurs[29] when $B \gtrsim K(m_c^* c\epsilon_g^2/\hbar e\epsilon_F)$ or when $\hbar\omega_c\epsilon_F/\epsilon_g^2 \gtrsim K$, where ϵ_g is the energy of the potential barrier, and K is a quantity that depends on the geometry of the FS and is of the order of 1. The areas C, L, and T, also encircled by MB orbits, are graphed in Fig. 5.

Subscripts on the letter symbols distinguish the three principal crystal planes in which $\vec{B}$, normal to the area, was oriented. The superscripts distinguish different extremal cross sections. Figure 4(a) identifies the extremal cross sections μ_1^1, μ_1^2, and μ_1^5 of the monster for $\vec{B}$ in the [1120]-[0001] plane, oriented 60° from the c axis. Corresponding to these cross sections are the extremal cross sections of the diagonal arms μ_2^1, μ_2^2, and the waist μ_2^4, when $\vec{B}$ is in the [10$\bar{1}$0]-[0001] plane. The cross sections μ_3^2 and μ_3^3 are through the waist of the monster when $\vec{B}$ is in the basal plane. The symbols used in Figs. 3–5 and in Table I have the same significance as in Stark's[9] paper.

The areas graphed in Fig. 3 were determined from measurements of $\Delta(1/B)$ periods. These area determinations were made at 2° intervals in the orientation of $\vec{B}$ up to 8° from a principal crystal axis and at 4° intervals for larger angles. The ranges of the curves indicate the ranges of orientation of $\vec{B}$ over which oscillations were measurable.

In Table I are listed the extremal areas normal to the three principal crystal axes that we observed together with an estimate of our precision of determination based on the scatter of the observations. Values reported by Stark[9] are also given.

The differences in areas of extremal cross sections determined using the beat periods are in good agreement with the differences in Stark's[9] paper. These included the beating pairs μ_1^1 and μ_1^2, μ_2^1 and μ_2^2, L_1^1 and L_1^2, L_2^1 and L_2^2, and A and $A+\gamma$. The frequencies of the component oscillations of these beats were assumed to be symmetrically placed with respect to the carrier frequency $\nu_{\text{carrier}} = \frac{1}{2}(\nu_1+\nu_2)$ in accordance with the assumption that the component oscillations were of equal amplitude. The extremal areas listed in Table I for the μ_1^1, μ_1^2, μ_2^1, L_1^1, L_1^2, A, and $A+\gamma$ oscillations are in good agreement with Stark's[9] values. In the case of the A-$(A+\gamma)$ pair, this agreement was unexpected because the amplitude at the beat nodes

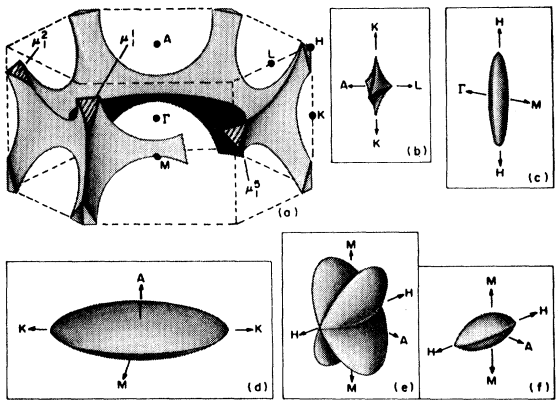

FIG. 4. Diagrams of six different types of sections (sheets) of the FS of Mg reduced to the first Brillouin zone: (a) monster (second-zone holes); (b) cap (first-zone holes); (c) cigar (third-zone electrons); (d) lens (third-zone electrons); (e) butterfly (third-zone electrons); (f) (fourth-zone electrons). The normals to the cross sections μ_1^1, μ_1^2, and μ_1^5 of the monster in (a) are oriented 60° from the [0001] axis in the [11$\bar{2}$0]-[0001] plane.

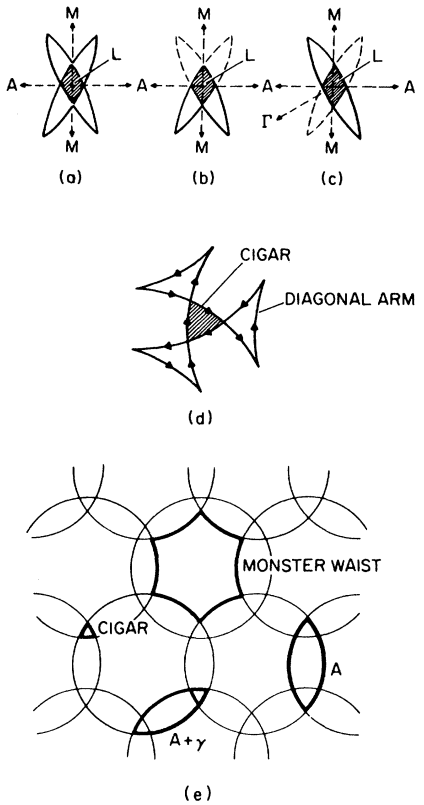

FIG. 5. Magnetic-breakdown coupled orbits: (a) cross section of a third-zone butterfly and a fourth-zone electron pocket (shaded portion) in absence of MB; (b) clamlike C orbit resulting from MB between butterfly and fourth-zone pocket; (c) lenslike L orbit resulting from MB between butterfly and fourth-zone pocket; (d) MB T orbits between three second-zone diagonal arms of the monster and third-zone cigar; (e) MB orbits between monster waist and cigar.

for this pair was not small. Beats of the T_1^1 and γ_1^1, and T_2^1 and γ_2^1 pairs were observed that exhibited a characteristic feature of MB: At low fields (< 12 kG) the amplitudes of the γ oscillations exceeded the amplitudes of the T oscillations, whereas at high fields (> 18 kG) the order was reversed. The areas for the component γ and T oscillations were determined from the periods of the component oscillations dominant in the high- and low-field regions.

Stark[9] measured some extremal areas that we did not; for example, we did not observe the α cross sections belonging to the first-band hole pocket called the cap in Fig. 4(b). Stark did not observe this cross section at fields greater than 3.1 kG because of MB which converted electron orbits around the cap into orbits around (cap + monster). The lowest field at which we could clearly observe magnetoacoustic oscillations with our specimens was 5 kG because of the lower purity of our Mg. In the range of cross-sectional areas 0.02–0.07 a.u. Stark observed[30] several areas, closely spaced, that we did not identify. These included sections through the arms and midsection of the monster and areas with MB between the monster and cigar. We were not able to analyze and to separately identify the components of a mixture of three or more oscillations if these were of comparable amplitude. Because the cutoff of our bandpass filters was not sharp, it was not possible to isolate with the filters oscillations with frequencies $\nu_1/\nu_2 < 2$ if they were of comparable amplitude. Also, it was not possible to isolate the weak member of a strong-weak pair of oscillations if $\nu_1/\nu_2 < 5$. The nonuniformity of the magnetic field of our superconducting magnet ($< 10^{-4}$ over a sphere 2.5 cm in diameter at the center) was not a limitation on the observation of extremal areas less than 0.4 a.u. There is no reason growing out of our investigation for not thinking that all the extremal areas measured by Stark[9] are magnetoacoustically active. We believe that they were not all observed by us because of the limitation on the ability of our apparatus to resolve a complex mixture of frequencies. Perhaps if our Mg had been purer and the amplitudes of the magnetoacoustic

TABLE I. Extremal areas perpendicular to a crystal axis.

Cross section	Crystal axis	Extremal areas in a.u. From present magnetoacoustic investigation[a]	From dHvA data by Stark[b]
$\mu_1^1, \mu_1^2, \mu_2^1, \mu_2^2$	[0001]	$(2.18 \pm 0.03) \times 10^{-3}$	2.15×10^{-3}
μ_1^1, μ_3^1	$[11\bar{2}0]$	$(4.0 \pm 0.1) \times 10^{-3}$	4.09×10^{-3}
μ_2^1, μ_3^1	$[10\bar{1}0]$	$(5.0 \pm 0.2) \times 10^{-3}$	5.12×10^{-3}
μ_1^5, μ_2^3	$[11\bar{2}0]$	$(7.04 \pm 0.07) \times 10^{-3}$	7.21×10^{-3}
μ_2^4, μ_2^3	$[10\bar{1}0]$	$(8.45 \pm 0.08) \times 10^{-3}$	8.45×10^{-3}
μ_3^3	$[10\bar{1}0]$	$(8.3 \pm 0.2) \times 10^{-3}$	8.45×10^{-3}
γ_1^1, γ_2^1	[0001]	$(6.05 \pm 0.06) \times 10^{-3}$	5.98×10^{-3}
λ_1^1, λ_3^1	$[11\bar{2}0]$	$(7.21 \pm 0.07) \times 10^{-2}$	7.27×10^{-2}
λ_2^1, λ_3^1	$[10\bar{1}0]$	$(7.22 \pm 0.07) \times 10^{-2}$	7.26×10^{-2}
C_1^1	$[11\bar{2}0]$	$(2.3 \pm 0.4) \times 10^{-2}$	2.08×10^{-2}
C_1^2	$[11\bar{2}0]$	$(3.1 \pm 0.4) \times 10^{-2}$	3.12×10^{-2}
$L_1^1, L_1^2, L_2^1, L_2^2$	[0001]	$(2.33 \pm 0.04) \times 10^{-2}$	2.34×10^{-2}
T_1^1, T_2^1	[0001]	$(6.36 \pm 0.07) \times 10^{-3}$	6.34×10^{-3}
A	[0001]	$(1.43 \pm 0.02) \times 10^{-1}$	1.44×10^{-1}
$A+\gamma$	[0001]	$(1.50 \pm 0.02) \times 10^{-1}$	1.50×10^{-1}

[a] ± values are estimated limits of uncertainty.
[b] Areas given by Stark (Ref. 9) have an "accuracy" of 0.5%.

oscillations in consequence larger, we would have had a better change of separating and identifying mixtures of more than two oscillations.

All our data in Table I and Fig. 3 are in agreement with Stark[9] to within the limits of uncertainty of the two investigations (1.5%) with one exception, namely, the $\mu_1^5(\mu_3^2)$ area perpendicular to the $[11\bar{2}0]$ axis. Our value for this area $(7.04 \pm 0.01) \times 10^{-3}$ a.u. (see Table I) is based on 15 different observations using four specimens. Stark's[9] value, 7.21×10^{-3} a.u., $\pm 0.5\%$, is larger than our value. The mean deviation of our observations was 0.01×10^{-3} a.u. and the accuracy of the mean 1%. As Stark's Mg was much purer than ours ($R_{300}/R_4 \sim 2.5 \times 10^4$ vs ~425 for our specimens), impurities in our specimens were suspect. While this explanation cannot be ruled out on the basis of our work, it is not supported by our results either. For example, other cross sections of the monster of small size that would be expected to be similarly affected by impurities are in good agreement with Stark's values. We were bothered by small errors in the orientation of our specimens (up to 3° maximum), but because the $\mu_1^5(\mu_3^2)$ area is a minimum along the $[11\bar{2}0]$ axis, misorientation of the specimen can result only in increased values of the area, whereas our value is smaller than Stark's. Because the $\mu_1^5(\mu_3^2)$ area is well separated from other extremal areas perpendicular to the $[11\bar{2}0]$ axis, this area could be measured with high accuracy. It is interesting that the $\mu_1^5(\mu_3^2)$ area perpendicular to the $[11\bar{2}0]$ axis calculated by Kimball, Stark, and Mueller[2] using their nonlocal pseudopotential for Mg, based on empirical magnetoacoustic absorption and dHvA data, is 7.07×10^{-3} a.u. in close agreement with our Table I value 7.04×10^{-3} a.u.[31]

The oscillations in $\alpha(B)$ arising from the λ_1^1 and λ_2^1 areas were amplitude modulated, λ_1^1 with the μ_1^5 frequency and λ_2^1 with μ_2^4. The λ areas being large, their $\alpha(B)$ oscillations are of small amplitude in accordance with theory, and, in fact, the λ oscillations were not measurable below 30 kG. Between 30 and 40 kG, there is a 10% modulation of the amplitude of the λ oscillation that does not change with B, although the amplitude of the λ oscillation increases with B as predicted by Eqs. (8) and (12). The $\alpha(B)$ oscillations have the appearance of beats between a λ oscillation and a MB oscillation for an extremal area of $(\lambda_1^1 + \mu_1^5)$ or $(\lambda_2^1 + \mu_2^4)$. However, this is ruled out as a likely possibility, at least for a $(\lambda_2^1 + \mu_2^4)$ area, because the extremal areas λ_2^1 (through the lens) and μ_2^4 (across the waist of the monster) perpendicular to the $[10\bar{1}0]$ axis lie in different (noncoincident but parallel) planes making impossible one cyclotron orbit around both areas. The possibility of the generation of combination frequencies in the electronic receiver because of nonlinear responses was considered because we were aware of a small nonlinearity in the gated integrating amplifier. The amplitudes of the μ_1^5 and μ_2^4 oscillations, being an order of magnitude larger than the amplitudes of the λ_1^1 and λ_2^1 oscillations, make the generation of a small-amplitude combination frequency seem a possibility. However, we do not think this is plausible because we do not observe the phenomenon where other small-amplitude oscillations occur in the presence of large oscillations. We think this is an interesting phenomenon requiring further investigation.[32]

B. Amplitudes of Magnetoacoustic Oscillations

A limited investigation showed that Eqs. (8) and (12) represent quite well the dependence of the amplitude of the MA oscillations in Mg on the parameters B, T, q, and $\theta \equiv \angle \vec{q}, \vec{B}$, in spite of the simple assumption on which these equations are derivable. For this investigation, the ultrasonic apparatus was calibrated so that changes in the heights of echo pulses were measurable in decibels. The check made was not precise.

The factor $\alpha_{ij}(\vec{q}, l, \vec{B} \to 0)$ on the right-hand side of Eq. (12), the mean value of the MA attenuation about which $\alpha_{ij}(B)$ oscillates, was regarded as being independent of B. We found for our Mg specimens ($\omega\tau \sim 2 \times 10^{-4}$) that $\alpha(\vec{q}, l, \vec{B} \to 0)$ was approximately independent of B (0–40 kG) and of T (1–4.2 K) to within ~2%, or $\pm 1\frac{1}{2}$ dB in 70 dB for θ between 50° and 90°. Between 0° and 50° α decreases ~0.08 dB/deg for a total change of ~4 dB in 70 dB.

For the intermediate region $\sqrt{2} q_z l > 1$, Eq. (12) predicts that the amplitude of the $\alpha_{ij}(B)$ oscillation is proportional to $q_z l$, if $|q|$ and the direction of $\vec{B}$ are fixed. For $\vec{q}$ along a principal crystal axis (a necessary requirement for pure longitudinal waves) and $\vec{B}$ constant, we expect that

$$\text{amp}\,\alpha_{ij}(B, \theta = 0)/\text{amp}\,\alpha_{ij}(B, \theta = \tfrac{1}{2}\pi) = \sqrt{2} q_z l$$

if $\sqrt{2} q_z l > 1$ and equal to 1 if $\sqrt{2} q_z l \leq 1$. At $\theta = \frac{1}{2}\pi$, we are in the dHvA region. Using the μ_1^1 oscillation, we observed with $\vec{B}$ fixed along the [0001] axis and $\vec{q}$ first along the [0001] and then the $[11\bar{2}0]$ axis that $\text{amp}\,\alpha_{\mu_1^1}([0001])/\text{amp}\,\alpha_{\mu_1^1}([11\bar{2}0])$ was the order of 1 as expected since $\sqrt{2} ql$ was ~1.8. The μ_1^1 periods for these two orientations of $\vec{q}$ were the same.

According to Eq. (12), the ratio of the amplitudes of the $\alpha_{ij}(B)$ oscillations at different T's for the same $\vec{B}$ is determined by the cyclotron mass m_{ci}^*. This was checked by using the μ_1^5 oscillation with B equal to 23 kG and $\vec{B}$ and $\vec{q}$ parallel to the $[11\bar{2}0]$ axis. At 260 MHz, we obtained for m_c^*/m, 0.14 ± 0.08 when $2.17\ \text{K} < T < 4.2$ K, and 0.138 ± 0.010 when $1\ \text{K} < T < 2.17$ K; and, at 300 MHz, 0.145 ± 0.08 when $2.17\ \text{K} < T < 4.2$ K, and 0.138 ± 0.007 when $1\ \text{K} < T < 2.17$ K. Stark's[9] value, derived from the dHvA effect, was 0.138.

TABLE II. Comparison of measured amplitudes $\Delta\alpha$ of the μ_1^5 oscillation with $\psi(ql)$ amd $ql\psi(ql)$ at different sonic frequencies.[a]

Frequency (MHz)	ql for μ_1^5	$\Psi(ql)$	$ql\Psi(ql)$	$\Delta\alpha$ (dB)	Ratios of $\Delta\alpha$'s		Ratios of $\Psi(ql)$'s		Ratios of $ql\Psi(ql)$'s	
300	1.27	0.327	0.415	3.0	1.0	4.8	1.0	7.1	1.0	21.0
260	1.10	0.258	0.284	2.0	0.67	3.1	0.85	5.1	0.68	14.0
180	0.765	0.138	0.105	1.0	0.33	1.6	0.42	3.0	0.253	5.2
100	0.425	0.046	0.020	0.62	0.21	1.0	0.141	1.0	0.048	1.0

[a] $\Psi(ql)$ is defined by Eq. (2).

The ratio of $\alpha_{ij}(B)$ amplitudes at different B's for the same T determines[19] the Dingle temperature, $T_{Dij}=\hbar/2\pi k_B\tau_{ij}$. With $\vec{B}$ and $\vec{q}$ parallel to the $[11\bar{2}0]$ axis and $T=1.0$ K, we obtained (1.3 ± 0.5) K for $T_D(\mu_1^5)$ and 9×10^{-13} sec for $\tau(\mu_1^5)$. The electrical conductivity τ_σ for our Mg was 4×10^{-12} sec using $m^*/m=1$, and 5×10^{-12} sec using the electronic specific-heat[33] determined ratio $m^*/m=1.33$. Thus, $\tau(\mu_1^5)/\tau_\sigma\sim0.2$, which is reasonable.

Brailsford[34] discussed the relation of τ for cyclotron states to τ_σ calculated from the electrical conductivity on the assumption that the conductivity scattering is isotropic. In general, the scattering of electrons in cyclotron motion is not isotropic, and differs from one extremal cross section to another. Roughly, $\tau/\tau_\sigma\sim\langle1-\cos\theta\rangle_{av}$, where the average of $(1-\cos\theta)$ is over the scattering angle θ for cyclotron motion. In general, there is a preponderance of small-angle scattering for cyclotron motion making $\tau/\tau_\sigma<1$. For metals, chemically very pure, τ is far more sensitive to dislocations than is τ_σ, so that τ/τ_σ can be very small for very pure metals.[35]

The dependence of the oscillation amplitude on q (or ql) was investigated using the μ_1^5 oscillation. Amplitudes at 100, 180, 260, and 300 MHz were measured at 1 K, with $B=23$ kG and $\vec{B}$ and $\vec{q}$ parallel to the $[11\bar{2}0]$ axis. In Table II, the ratios of the amplitudes of the μ_1^5 oscillations, in decibels, are compared with ratios of $\psi(ql)$ [see Eq. (2)] and $ql\,\psi(ql)$. The mean free path $l=4\times10^{-5}$ cm was obtained using $\tau(\mu_1^5)$ and $m_c^*(\mu_1^5)$ from above. For a spherical FS, the amplitude of the $\alpha(B)$ oscillation is proportional to $\psi(ql)$ in the dHvA region, and to $ql\psi(ql)$ in the intermediate region. The two regions meet at $\sqrt{2}q_z l\sim1$ or $q_z l\sim0.7$. The observations at 300 and 260 MHz ($ql>0.7$) fit $ql\psi(ql)$ better than they fit $\psi(ql)$. The 180-MHz observation fits the transition between the dHvA and intermediate regions, and the 100-MHz observation fits the dHvA region.

ACKNOWLEDGMENTS

The authors wish to thank Professor Eugen Skudrzyk for helping us get started in this investigation and for his continued encouragement, Dr. John de Klerk (Westinghouse Research Laboratories) and Dr. Bernard Droney (Bethlehem Steel Homer Research Laboratories) for helpful suggestions with respect to the apparatus, David E. Binnie for helping with the observations, and Professor George D. Whitfield for helpful discussions.

*Paper based on the thesis submitted by Robert W. Reed in partial fulfillment of the requirements for the Ph. D. degree.

†Work supported by the Ordnance Research Laboratory of the Pennsylvania State University under contract with the U. S. Naval Ordnance Systems Command.

[1]Three large single crystals of Mg were kindly supplied by Dr. R. S. Busk, Director of the Metallurgical Laboratory of the Dow Metal Products Co. We are grateful to Dr. Busk and the Dow Metal Products Co.

[2]J. C. Kimball, R. W. Stark, and F. M. Mueller, Phys. Rev. 162, 600 (1967).

[3]W. L. Gordon, A. S. Joseph, and T. G. Eck, in *The Fermi Surface*, edited by W. A. Harrison and M. B. Webb (Wiley, New York, 1970).

[4]M. G. Priestley, Proc. Roy. Soc. (London) A276, 258 (1963).

[5]R. W. Stark, T. G. Eck, and W. L. Gordon, Phys. Rev. 133, 443 (1964).

[6]M. G. Priestley, L. M. Falicov, and G. Weisz, Phys. Rev. 131, 617 (1963).

[7]E. W. Fenton and S. B. Woods, Phys. Rev. 151, 424 (1966).

[8]J. B. Ketterson and R. W. Stark, Phys. Rev. 156, 748 (1967).

[9]R. W. Stark, Phys. Rev. 162, 589 (1967).

[10]V. L. Gurevich, V. G. Skobov, and Yu. A. Firsov, Zh. Eksperim. i Teor. Fiz. 40, 786 (1961) [Soviet Phys. JETP 13, 552 (1961)].

[11]S. H. Liu and A. M. Toxen, Phys. Rev. 138, 487 (1965).

[12]V. G. Skobov, Zh. Eksperim. i Teor. Fiz. 40, 1446 (1961) [Soviet Phys. JETP 13, 1014 (1961)].

[13]J. J. Quinn and S. Rodriguez, Phys. Rev. 128, 2487 (1962).

[14]A. B. Pippard, *The Dynamics of Conduction Electrons* (Gordon and Breach, New York, 1965), Chap. XI.

[15]Reference 14, p. 120, Eq. (192).

[16]Reference 7; Eq. (5) in this reference is similar to our Eq. (4).

[17]J. M. Ziman, *Principles of the Theory of Solids* (Cambridge U. P., London, 1964), pp. 278–9.

[18]Reference 14, pp. 21–22.

[19]A. D. Brailsford, Phys. Rev. 149, 456 (1966), Eq. (23).

[20]Reference 19, Eq. (40).

[21]Reference 19, Eq. (31).

[22]The design of our apparatus was influenced by a design of J. B. Ketterson and Y. Eckstein, Rev. Sci. Instr. 37, 44 (1966).

[23]R. W. Reed and F. G. Brickwedde, Rev. Sci. Instr. 39, 1216 (1968).

[24]This circuit was adapted from D. F. Gibbons and L. M. Falicov, Phil. Mag. 8, 177 (1963).

[25]R. Maddin and W. R. Asher, Rev. Sci. Instr. 21, 881 (1950).

[26]M. Levy and I. Rudnick, J. Acoust. Soc. Am. 34, 520 (1962).

[27]The field of the superconducting magnet in air and liquid helium is described by H, measured in oersteds. The conduction electrons in the specimen respond to B, measured in gauss. It was assumed that the relative permeability μ of Mg and the apparatus inside the superconducting solenoid was 1.

[28]The relation between the magnetoacoustic period $\Delta(1/B)$ and the corresponding extremal area S it measures is $\Delta(1/B) = 2\pi e/c\hbar S$ or $s_m = 2.673 \times 10^{-7} \Delta(1/B)$, if s_m is in a.u. and $\Delta(1/B)$ is in G^{-1}.

[29]R. W. Stark and L. M. Falicov, in *Progress in Low Temperature Physics*, edited by C. J. Gorter (North-Holland, Amsterdam, 1967), Vol. V, Chap. VI, pp. 235–286.

[30]Stark (Ref. 9) identified component frequencies of complex mixtures of harmonic oscillations in the dHvA effect using the field-modulation technique described by R. W. Stark and L. R. Windmiller, Cryogenics 8, 272 (1968).

[31]Dr. Stark has informed us that he has checked his determination of the μ_1^5 area and concluded that his original value is correct.

[32]Dr. Stark informed us that he also had observed this modulation of the λ oscillations in the dHvA effect.

[33]S. A. Friedberg, I. Estermann, and J. E. Goldman, Phys. Rev. 85, 375 (1952); 87, 582 (1952).

[34]Reference 19, Part IV.

[35]R. A. Phillips and A. V. Gold, Phys. Rev. 178, 932 (1969).

PHYSICAL REVIEW B VOLUME 3, NUMBER 4 15 FEBRUARY 1971

Ultrasonic Quantum Oscillations in Chromium†

D. F. Snider*‡§ and R. L. Thomas
Department of Physics, Wayne State University, Detroit, Michigan 48202
(Received 13 August 1970)

Measurements of quantum oscillations in the ultrasonic attenuation have been made to investigate the Fermi surface of chromium in the "single-$\vec{Q}$" state. Several frequency branches were followed over the entire Fermi surface and many of these data agree with earlier de Haas–van Alphen and ultrasonic results. Three branches display harmonic behavior which is exact when the measuring field is in the basal plane, but which deviates smoothly from exactness as the field is rotated toward $\vec{Q}$. The most likely explanation of this feature is that of magnetic breakdown among nonextremal orbits on the Fermi surface. The lack of degeneracy of the branches at certain symmetry axes prevented identifying the data with the location of sections of the Fermi surface. The data in one family of branches agree point by point with the de Haas–van Alphen results when the measuring field is near the basal plane, but differ as the field approaches $\vec{Q}$. For the remaining data, symmetry arguments may not be applicable because of changes in the topology caused by magnetic breakdown.

I. INTRODUCTION

The antiferromagnetic ground state of chromium has been successfully explained[1] in terms of spin-density wave (SDW) theory.[2] A central feature of this description is that the wave vector $\vec{Q}$ of the SDW is incommensurate with the lattice periodicity, and that a number of energy gaps are introduced into the band structure, giving rise to drastic changes in the Fermi-surface topology from that predicted for the paramagnetic state.

Below the Néel temperature T_N and without external constraints, the magnetic structure of normal chromium is cubic. However, if a relatively strain-free crystal is cooled through the Néel temperature in the presence of a sufficiently large magnetic field, only one SDW appears which is along the [100] axis nearest in orientation to the cooling field.[3,4] This is usually called the "single-$\vec{Q}$" state. In the temperature region $T_{sf} < T < T_N$ and in the presence of a magnetic field, chromium displays orthorhombic symmetry.[5,6] Here, T_{sf} is the spin-flip temperature at which the polarization of the SDW changes from transverse to longitudinal.[7] Below T_{sf}, chromium's magnetic symmetry is tetragonal, with fourfold rotational symmetry about

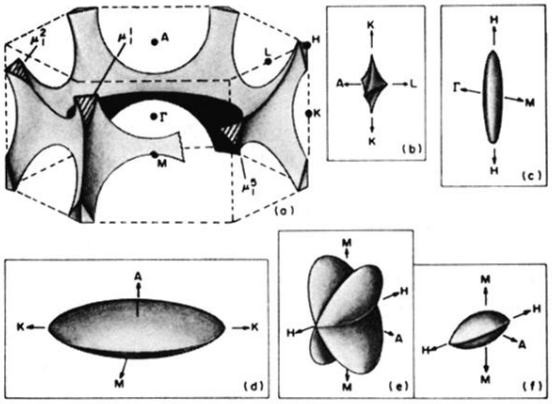

FIG. 4. Diagrams of six different types of sections (sheets) of the FS of Mg reduced to the first Brillouin zone: (a) monster (second-zone holes); (b) cap (first-zone holes); (c) cigar (third-zone electrons); (d) lens (third-zone electrons); (e) butterfly (third-zone electrons); (f) (fourth-zone electrons). The normals to the cross sections μ_1^1, μ_1^2, and μ_1^5 of the monster in (a) are oriented 60° from the [0001] axis in the $[11\bar{2}0]$-[0001] plane.